Graph-Based Geometric-Iconic Guide-Wire Tracking

Nicolas Honnorat[1,2,3], Régis Vaillant[1], and Nikos Paragios[2,3,⋆]

[1] General Electric Healthcare, Buc, France
[2] Laboratoire MAS, Ecole Centrale Paris, Châtenay-Malabry, France
[3] Equipe GALEN, INRIA Saclay-Ile-de-France, Orsay, France

Abstract. In this paper we introduce a novel hybrid graph-based approach for Guide-wire tracking. The image support is captured by steerable filters and improved through tensor voting. Then, a graphical model is considered that represents guide-wire extraction/tracking through a B-spline control-point model. Points with strong geometric interest (landmarks) are automatically determined and anchored to such a representation. Tracking is then performed through discrete MRFs that optimize the spatio-temporal positions of the control points while establishing landmark temporal correspondences. Promising results demonstrate the potentials of our method.

Keywords: Guide-wire, tracking, MRF, simultaneous geometric-iconic registration, landmarks matching.

1 Introduction

Several works tried to address the tracking of the guide-wires (GW) used during cardiac angioplasty interventions for positioning surgical devices into the artery to be cured, because a reliable localization of these wires would be valuable for the intervention monitoring and assistance. This task inherits unfortunately important technical and theoretical challenges. Although the tip of these wires is usually made of a more absorbent material, the main part of these wires is often barely detectable for conventional curvilinear operators [2]. The detection literature provides numerous alternatives, such as Hessian regularized by coherence enhancing diffusion [1], Vesselness [6] and phase congruency [12]. Boosted detectors combining Haar features or steerable filters and image statistics have been used recently [14,7] but these better detectors are more complex or time consuming. The second challenge is related to the large and unforeseeable motion of the GW, due to the combination of cardiac/respiratory motions and patient displacement. Their accumulation cannot be easily captured using conventional prediction mechanisms. Most of the existing tracking approaches represent GW

⋆ This work was supported by ANRT (grant 1062/2008), GE Healthcare and the European Research Council Starting Grant Diocles (ERC-STG-259112). The authors thank T. Hauke Heibel, the reviewers and S. Bernhardt for their help and comments.

G. Fichtinger, A. Martel, and T. Peters (Eds.): MICCAI 2011, Part I, LNCS 6891, pp. 9–16, 2011.

with B-splines which optimal displacement is found through optimization. In [1] Powell's direction set method was used for tracking rigid GW tips while [14] proposed a method carrying out a rigid alignment followed by a non-rigid registration displacing control-points.

Other GW tracking methods can be associated with well-known contour tracking algorithms. The B-spline snakes have thus been exploited in [12] with an external energy driven from X-ray phase congruency, an internal energy favoring low curvature and a length prior. Methods based on dynamic programming and graphical models were also investigated. The space of possible displacements was for instance discretized and optimal ones were determined using dynamic programming. The CONDENSATION algorithm [8] was applied successfully to tracking contours represented with B-splines. Nevertheless, the space of contour localizations was reduced to a shape space. A parametrized curve tracker based on a Markov Random Field (MRF) framework was recently proposed in [6] and improved in [11]. The main advantage of these approaches is that they achieve near-optimal solution at reasonable computational complexity.

Our approach lies within this scope. First, we address the low signal-to-noise ratio by using steerable filters designed for ridge detection [9] that are enhanced by tensor voting [4,3]. Toward coping with important displacements, we introduce a unified framework which combines an iconic B-spline tracking [6] with a landmark matching approach [13]. We improve the iconic part by using a data term more robust with respect to false GW detections and a prior penalizing also wires rotations. The resulting formulation recovers both landmarks position and the GW displacements through the use of image support and spatio-temporal consistency. This is achieved through a two-part graph acting on the two sets of variables which are coupled in a rigorous mathematical manner. The overall formulation is solved using efficient linear programming.

2 Hybrid Curve Tracking

Iconic tracking methods allow to track non-rigid structures precisely but can be sensitive to local minima (due to erroneous image support) and, depending on the optimization schema, can fail to account for large displacements.

On the contrary, geometric methods rely on the matching of salient structures and can therefore deal with large displacements efficiently. On the other hand, deformations are sparse and incomplete since information for the motion/displacement of the structure between landmark points is not recovered.

Tracking GW during cardiac interventions involves large displacements and non-rigid deformations. Hence we propose a unified discrete framework like [13] combining a variant of the iconic tracking of [6] with a geometric tracking relying on landmarks extracted along the GW. This framework also model exactly the interaction between these two parts. Without loss of generality, let us first consider a representation of the wire with N control-points $\mathbf{c}(i)$ and a set of M landmarks $\mathbf{p}(j)$ extracted along the wire. These variables evolve in time towards representing the structure of interest, or $\mathcal{X}(t) = \{\mathbf{c}(i;t), \mathbf{p}(j;t)\}$.

In terms of support, let us consider a vectorial feature image where measurements of the strength $g(\mathbf{x};t)$ and the orientation $\theta(\mathbf{x};t)$ of the GW are combined: $\mathcal{F}(t) = \{g(\mathbf{x};t)cos(\theta(\mathbf{x};t)), g(\mathbf{x};t)sin(\theta(\mathbf{x};t)\}$. Let us also consider that for the different landmark points $\mathbf{p}(j;t)$, candidate correspondences have been determined at the frame $t+1$ denoted with $\mathcal{P} = \{\mathbf{p}^L(j;m;t+1)\}$, where L is the number of candidates per landmark and $m \in \{1 \dots L\}$. GW tracking is then equivalent to finding the optimal configuration for $\mathcal{X}(t+1)$, given $\mathcal{X}(t)$, $\mathcal{F}(t+1)$ and $\mathbf{p}^L(j;m;t+1)$.

We adopt a unified first order MRF framework combining unary and pairwise potentials involving either the displacements l_i of $\mathbf{c}(i;t)$ or the matching l_j of $\mathbf{p}(j;t)$, originated from data, prior, landmarks and coupling terms:

$$E_{MRF} = \sum_{x \in \left\{ \begin{smallmatrix} data,\ landmarks, \\ template,\ coupling \end{smallmatrix} \right\}} \mu_x \left(\sum_{k \in \{i,j\}} V_k^x(l_k) + \sum_{k,r \in \{i,j\}} V_{k,r}^x(l_k, l_r) \right)$$

2.1 Iconic Graph-Based Curve Tracking

The iconic part of our framework extends the MRF-based curve tracking method proposed in [6]. We represent the curve with a cubic B-spline based on points $\mathbf{c}(i;t)$ and we build an MRF graph containing one node per control point. We discretize the space of admissible displacements of each $\mathbf{c}(i;t)$ and denote with $\mathbf{v}(l_i)$ the admissible displacement associated with label l_i chosen for $\mathbf{c}(i;t)$. [Fig. (2)] illustrates this procedure. Like [6], let us note with $N_i(.)$ the basis function of each control point, $s \in [0,1]$ the curvilinear abscissa along the spline and $N_{i,i+1}(.)$ the following influence function: $N_{i,i+1}(s) = \frac{N_i(s)N_{i+1}(s)}{\sum_k N_k(s)N_{k+1}(s)}$. The spline curve $\mathcal{C}(s)$ is given by: $\mathcal{C}(s) = \sum_i N_i(s)\mathbf{c}(i;t)$. Let us denote with $C(s, l_i, l_{i+1})$ the curve obtained when the control points $\mathbf{c}(i;t)$ and $\mathbf{c}(i+1;t)$ are displaced by $\mathbf{v}(l_i)$ and $\mathbf{v}(l_{i+1})$ respectively (and similarly $C'(s, l_i, l_{i+1})$ its derivative), let us denote with $< .,. >$ the standard scalar product. In order to introduce the image support term, we consider the following exponential function: $\psi(x) = e^{-\gamma x}$.

We adopt two sums of pairwise potentials. The first forces the curve towards pixels likely to be part of the structure (the strength of the image support is important and the tangent of the curve is coherent with the local image orientation [1]),with $s(\mathbf{c}(i;t))$ being the curvilinear abscissa of $\mathbf{c}(i;t)$:

$$V_{i,i+1}^{data}(l_i, l_{i+1}) = \int_{s(\mathbf{c}(i;t))}^{s(\mathbf{c}(i+1;t))} \psi\left(\frac{| < C'(s, l_i, l_{i+1}), \mathcal{F}(C(s, l_i, l_{i+1}); t+1) > |}{||C'(s, l_i, l_{i+1})||} \right) ds$$

The second term penalizes the local changes of the curve derivatives with respect to a template $\mathcal{T}(s)$ corresponding to the form of the GW in the previous frames and updated using exponential forgetting: $\mathcal{T}(s) \leftarrow \frac{memory-1}{memory}\mathcal{T}(s) + \frac{1}{memory}C(s)$. It is more constraining than length preserving priors [12,6].

$$V_{i,i+1}^{template}(l_i, l_{i+1}) = \int_{s(\mathbf{c}(i;t))}^{s(\mathbf{c}(i+1;t))} \frac{||\epsilon\ C'(s, l_i, l_{i+1}) - \mathcal{T}'(s)||^2}{||\mathcal{T}'(s)||^2} ds$$

However, such an approach might require too many labels to deal with large displacements, can be sensitive to missing visual support and does not provide temporal understanding of the GW deformation. We introduced landmark matching into our framework for tackling these concerns.

2.2 Landmarks Matching

The landmark matching part of our system adopts a fully connected pairwise MRF, which optimal labeling indicates the candidates chosen for the matching. In order to increase the robustness and to deal with mis-detections or erroneous detections, we introduce a label $(L+1)$ corresponding to absent correspondences. We encoded a penalization of the deformation of the landmark configuration into the pairwise potentials. More precisely, the unary potentials were given by:

$$V_j^{landmarks}(l_j) = \begin{cases} K & if\ l_j = L+1 \\ 0 & otherwise \end{cases}$$

we chose the following potentials to penalize landmarks configurations changes:

$$V_{j,k}^{landmarks}(l_j, l_k) = \begin{cases} 0 & if\ l_j = L+1\ or\ l_k = L+1 \\ \min\left(||\mathbf{u}(j,l_j,k,l_k) - \mathbf{u}(j,k)||^2, \Gamma\right) & otherwise \end{cases}$$
$$\mathbf{u}(j,l_j,k,l_k) = \mathbf{p}^L(j;l_j;t+1) - \mathbf{p}^L(k;l_k;t+1)$$
$$\mathbf{u}(j,k) = \mathbf{p}(j;t) - \mathbf{p}(k;t)$$

This term aims at imposing geometric consistency between the location of landmarks in successive frames by considering their relative positions. The graph-matching cost increases with the Euclidean norm of the difference between the vector $\mathbf{u}(j,k)$ describing the configuration in the last frame and an admissible configuration $\mathbf{u}(j,l_j,k,l_k)$. If distances and orientations of landmarks pairs are preserved, then the cost is low. [Fig. (2)] presents example of matchings.

2.3 Coupled Markov Random Field for Hybrid Tracking

The hybrid model that we propose combines the two previous parts. The coupling term aims at imposing consistency between the iconic tracking and the geometric matching. As opposed to [13] where an approximation was used, we adopt an exact formulation that expresses consistency using singleton and pair-wise terms.

Let us denote with $\mathbf{w}_j(l_j)$ the displacement of the interest points $\mathbf{p}(j;t)$ corresponding to its matching with the candidate $\mathbf{p}^L(j;l_j;t+1)$ and with $s_j \in [0,1]$ its curvilinear abscissa. As in the previous section, $\mathbf{v}_i(l_i)$ denotes the displacement of the control point $\mathbf{c}(i;t)$ with respect to the frame t, and $N_i(.)$ the basis function of $\mathbf{c}(i;t)$. The following constraint is to be satisfied: $\sum_i N_i(s_j)\mathbf{v}_i(l_i) = \mathbf{w}_j(l_j)$ which imposes that the landmark displacement produced by the control points

motion is the same as the one determined from the matching. This constraint is converted into an energy term through penalization of the Euclidean distance:

$$E_j(\{l_i\}, l_j) = ||\sum_i N_i(s_j)\mathbf{v}_i(l_i) - \mathbf{w}_j(l_j)||^2 = \sum_{i \neq k} N_i(s_j)N_k(s_j) < \mathbf{v}_i(l_i), \mathbf{v}_k(l_k) > - 2\sum_i N_i(s_j) < \mathbf{v}_i(l_i), \mathbf{w}_j(l_j) > + \sum_i N_i(s_j)^2||\mathbf{v}_i(l_i)||^2 + ||\mathbf{w}_j(l_j)||^2$$

that converts the coupling constraint exactly into a sum of unary and pairwise potentials (contrary to [13] that minimizes only an upper bound of this energy).

Such an approach does not insure that the spline tracking will be guided by the geometric matching, since different displacements of the $\mathbf{c}(i;t)$ could lead to the same displacement of $\mathbf{p}(j;t)$. This can be easily addressed by adding pair-wise "rigidity" constraints to each landmark vicinity $v(j)$:

$$E_{r_j}(\{l_i\}) = \sum_{k \in v(j)} ||\mathbf{v}_k(l_k) - \mathbf{v}_{k+1}(l_{k+1})||^2$$

leading to the following coupling term:

$$\sum_k V_k^{coupling}(l_k) + \sum_{k,r} V_{k,r}^{coupling}(l_k, l_r) = \sum_j E_j(\{l_i\}, l_j) + \delta \sum_j E_{r_j}(\{l_i\})$$

3 Experimental Validation

In this section, we apply our approach to GW tracking in fluoroscopic sequences.

3.1 Steerable Filters Regularized by Tensor-Voting

We extracted the GW support with the most sensitive second order filter [9], which response is obtained (like Hessian response) by the eigen-decomposition of a matrix built using second order derivatives of the image. As we are interested in detecting dark structures, we considered the opposite of the main eigenvalue when it was negative (and a null response otherwise).

Towards improving their overall response, we used a fast variant of tensor voting (TV) introduced in [3]. Let us denote with $\hat{g}(\mathbf{x};t)$ and $\hat{\theta}(\mathbf{x};t)$ the response and the orientation provided by the steerable filter at location $\mathbf{x}$ in the frame t. We chose the following voting field (with notations [3], and we set $\sigma_{TV} = 4.5$):

$$V(r,\phi) = \frac{1}{16} e^{-\frac{r^2}{2\sigma_{TV}{}^2}} cos^4(\phi) \begin{pmatrix} 1 + cos(4\phi) & sin(4\phi) \\ sin(4\phi) & 1 - cos(4\phi) \end{pmatrix}$$

Like [3], we used this field to compute the new responses $g(\mathbf{x};t)$ and orientations $\theta(\mathbf{x};t)$, combined into the regularized field $\mathcal{F}(\mathbf{x};t)$:

$$\mathcal{F}(\mathbf{x};t) = (\mathcal{F}(\mathbf{x};t)_x, \mathcal{F}(\mathbf{x};t)_y) = (g(\mathbf{x};t)cos(\theta(\mathbf{x};t)), g(\mathbf{x};t)sin(\theta(\mathbf{x};t)))$$

[Fig. (1)] illustrates that the TV regularization clearly improves the results (contrary to the replacement of the Hessian by a steerable filter).

(i) 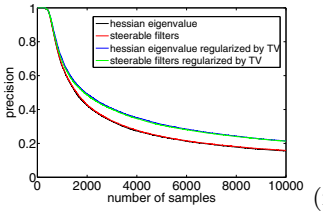

(ii) 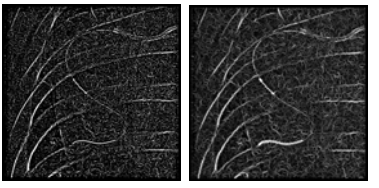

Fig. 1. (i) proportion of pixels extracted by Hessian and steerable filters regularized by TV belonging to the wire (estimated with 3 images by ranking pixels by decreasing filter response). (ii) norm of the steerable filter response and of the TV output.

3.2 Landmarks Extraction

Working with the regularized responses more reliable, we used the main eigenvalue of this tensor (inspired from structure tensor [5]) for landmarks detection:

$$T(\mathbf{x};t) = \sum_{\mathbf{y}} e^{-\frac{||\mathbf{x}-\mathbf{y}||^2}{2{\sigma_L}^2}} \begin{pmatrix} \mathcal{F}(\mathbf{y};t)_x^2 & \mathcal{F}(\mathbf{y};t)_x \mathcal{F}(\mathbf{y};t)_y \\ \mathcal{F}(\mathbf{y};t)_x \mathcal{F}(\mathbf{y};t)_y & \mathcal{F}(\mathbf{y};t)_y^2 \end{pmatrix}$$

This tensor favors pixels where strong and parallel responses accumulate. We set $\sigma_L = 2.5$. In order to take the local orientation into account when choosing the matching candidates $\mathbf{p}^L(j;m;t+1)$, we selected the L candidates $\mathbf{y}$ with the best matching scores (where $< .|. >$ denotes the inner product between matrices):

$$\mathscr{M}_j(\mathbf{y}) = < T(\mathbf{p}(j;t);t)|T(\mathbf{y};t+1) >$$

3.3 Implementation Details

First, we used a conventional multi-resolution strategy on the GW deformation search as suggested in [14]. We provided the spline at time 0 and the border of the field of view to our system and we forced the first control point to lie on this border if necessary. Besides, we updated the control points for keeping them equally distributed along the spline before processing every new frame in order to prevent a slow degeneracy of the spline. We made landmark detection more homogeneous along the GW by defining intervals of fixed length along the curve and choosing at most one landmark in each of them. FastPD [10] was used for minimizing E_{MRF}. We adressed abrupt elongations of the GW by elongating the tip of the curve in the direction of its tangent $\mathbf{d}$ before the control-points update. We appended pixels $\mathbf{q}$ while: $\psi(< \mathbf{d}, \mathcal{F}(\mathbf{q}) >) < 0.4$.

3.4 Validation

Validation was performed on 20 long fluoroscopic sequences of 200 frames of sizes between 512 and 1000 pixels covering a broad variety of clinical situations. The parameters were set using the first three sequences and performances were

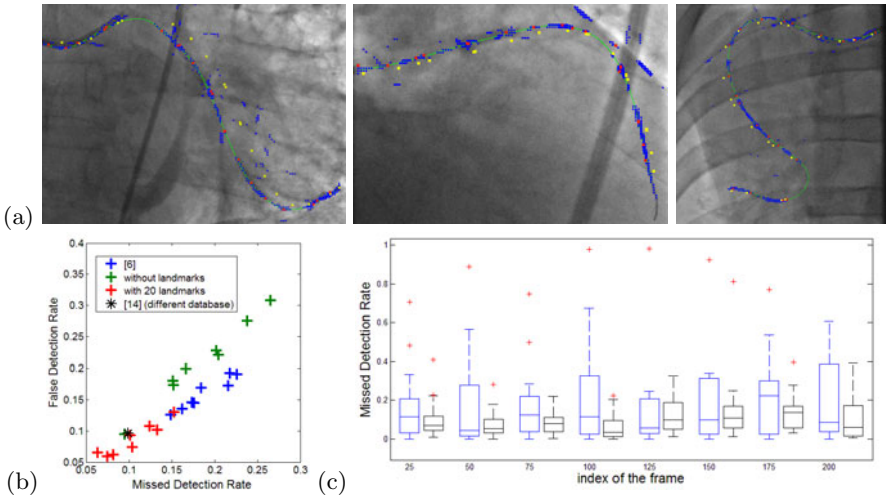

Fig. 2. (a) spline (green) landmarks detected along the previous spline (yellow) matching candidates (blue) and candidates chosen (red). (b) Mean tracking performances (measured every 25 frames for each experiment). [6] has been applied with a vesselness at scale 1.8 like our filters and $\lambda = 0.7$. The database for result [14] is different. (c) comparison of MDR obtained with [6] (blue boxes) and with our method (black boxes).

estimated on the other ones. We set $\mu_{data} = \mu_{template} = 1.0$, $\mu_{landmarks} = 2.10^{-4}$, $\mu_{coupling} = 3.10^{-5}$, $\delta = 0.1$, $\epsilon = 0.9$, $K = 45000$ for the landmarks not matched, displacements steps equal to $(25.0)2^{-\tau}$, $\tau \in \{0, \ldots 4\}$ and we sampled 25 displacements according to the sparse pattern [6]. We set $L = 24$, $\gamma = 6.10^{-3}$,$\Gamma = 500$ and $memory = 7$.

We measured missed detection rate (MDR) and false detection rate (FDR) for a distance of 5 pixels and for every 25 frames (2.5 seconds). These rates [14] correspond respectively to the proportion of pixels of the ground truth that lie too far from the spline and to the proportion of the spline that lie too far from the ground truth. [Fig. (2)] presents our results. [6] performs better than the iconic part of our model alone due to our worse displacement sampling and a different choice of initialization. Our complete method, however, outperforms [6] because the landmark matching both prevents the tracker from being mislead by local energy minima and preserves global spline configuration. We measured a distance between the tip of our tracker and the tip of the GW equal to 12.5 ± 11.5 pixels at the end of the sequences, what is acceptable since the GW tip is easy to locate. Our implementation processes one frame in 2 secondes (Intel Xeon 2.8 GHz) but would dramatically benefit from an adaptation to GPU.

4 Conclusion

In this paper we have presented a unified framework for geometric-iconic parametrized curves tracking. This novel framework achieves promising performances

on an extremely challenging task: the tracking of guide-wires in fluoroscopic sequences during cardiac angioplasty. One might investigate a GPU implementation achieving real-time and application of the method to a clinical setting. From a theoretical point of view, estimating uncertainties of the obtained solution might be helpful both for the quantitative interpretation of the result and for efficient parameterization of the search space. Another promising direction is to introduce long term memory through a dynamical system that could separate the different motion models.

References

1. Baert, S.A.M., Viergever, M.A., Niessen, W.J.: Guide-wire tracking during endovascular interventions. IEEE TMI 22(8), 965–972 (2003)
2. Frangi, A.F., Niessen, W.J., Vincken, K.L., Viergever, M.A.: Multiscale vessel enhancement filtering. In: Wells, W.M., Colchester, A.C.F., Delp, S.L. (eds.) MICCAI 1998. LNCS, vol. 1496, pp. 130–137. Springer, Heidelberg (1998)
3. Franken, E., van Almsick, M., Rongen, P., Florack, L.M.J., ter Haar Romeny, B.M.: An efficient method for tensor voting using steerable filters. In: Leonardis, A., Bischof, H., Pinz, A. (eds.) ECCV 2006. LNCS, vol. 3954, pp. 228–240. Springer, Heidelberg (2006)
4. Guy, G., Medioni, G.: Inferring global perceptual contours from local features. International Journal of Computer Vision 20, 113–133 (1996)
5. Harris, C.G., Stevens, M.J.: A combined corner and edge detector. In: 4th Alvey Vision Conference (1988)
6. Hauke Heibel, T., Glocker, B., Groher, M., Paragios, N., Komodakis, N., Navab, N.: Discrete tracking of parametrized curves. In: CVPR, pp. 1754–1761 (2009)
7. Honnorat, N., Vaillant, R., Paragios, N.: Guide-wire extraction through perceptual organization of local segments in fluoroscopic images. In: Jiang, T., Navab, N., Pluim, J.P.W., Viergever, M.A. (eds.) MICCAI 2010. LNCS, vol. 6363, pp. 440–448. Springer, Heidelberg (2010)
8. Isard, M., Blake, A.: Condensation conditional density propagation for visual tracking. IJCV 29 (1998)
9. Jacob, M., Unser, M.: Design of steerable filters for feature detection using canny-like criteria. IEEE PAMI 26(8), 1007–1019 (2004)
10. Komodakis, N., Tziritas, G., Paragios, N.: Performance vs computational efficiency for optimizing single and dynamic mrfs: Setting the state of the art with primal-dual strategies. CVIU 112, 14–29 (2008)
11. Pauly, O., Heibel, H., Navab, N.: A machine learning approach for deformable guide-wire tracking in fluoroscopic sequences. In: Jiang, T., Navab, N., Pluim, J.P.W., Viergever, M.A. (eds.) MICCAI 2010. LNCS, vol. 6363, pp. 343–350. Springer, Heidelberg (2010)
12. Slabaugh, G., Kong, K., Unal, G., Fang, T.: Variational guidewire tracking using phase congruency. In: Ayache, N., Ourselin, S., Maeder, A. (eds.) MICCAI 2007, Part II. LNCS, vol. 4792, pp. 612–619. Springer, Heidelberg (2007)
13. Sotiras, A., Ou, Y., Glocker, B., Davatzikos, C., Paragios, N.: Simultaneous geometric - iconic registration. In: Jiang, T., Navab, N., Pluim, J.P.W., Viergever, M.A. (eds.) MICCAI 2010. LNCS, vol. 6362, pp. 676–683. Springer, Heidelberg (2010)
14. Wang, P., Chen, T., Zhu, Y., Zhang, W., Zhou, S.K., Comaniciu, D.: Robust guidewire tracking in fluoroscopy. In: CVPR (2009)